Comparison of scanning laser annealing and microwave annealing for As^+ implanted Si

Zhao Zhao
School for Engineering of Matter, Transport, and Energy, Arizona State University, Tempe, Arizona 85287

Joe Hilman and Manny Oropeza
Universal Laser Systems, Scottsdale, Arizona 85260

Qiong Nian
School for Engineering of Matter, Transport, and Energy, Arizona State University, Tempe, Arizona 85287 and Birck Nanotechnology Center, Purdue University, West Lafayette, Indiana 47907

Terry L. Alford[a)]
School for Engineering of Matter, Transport, and Energy, Arizona State University, Tempe, Arizona 85287

(Received 14 September 2016; accepted 28 November 2016; published 16 December 2016)

Laser annealing and microwave (MW) annealing are rapid annealing techniques that can be used for postannealing of ion implanted semiconductors. In this study, laser annealing and MW annealing of As^+ implanted Si are compared in terms of dopant activation, energy absorption, recrystallization, and dopant diffusion. Laser annealing caused similar recrystallization and a slightly higher dopant activation than MW annealing did, at the same time, the energy density absorbed during laser annealing is ~1/7 lower than during MW annealing, due to surface heating. Rapid dopant activation and negligible dopant diffusion were achieved in the MW annealed sample. This indicates that MW annealing is a promising method for annealing ion implanted source, drain, and channel regions for shallow-junction transistor fabrication. On the other hand, laser annealing results in significant but uniform dopant diffusion, and therefore, laser annealing appears to be beneficial for quickly forming deep wells with uniform dopant concentrations for small scale wafer. © *2016 American Vacuum Society*. [http://dx.doi.org/10.1116/1.4972051]

I. INTRODUCTION

Metal-oxide-semiconductor field-effect transistors (MOSFETs) are indispensable as electronic devices. During the fabrication of MOSFETs, dopants including As^+, B^+, and P^+ are incorporated into Si wafers to alter the resistivity of the wafer surface and to define active regions of devices.[1–3] Dopants are incorporated by diffusion or ion implantation, with ion implantation being the more common method. Ion implantation is performed by accelerating ionized dopants to energies of 30–100 keV, and then implanting them into the wafer.[4] During the implantation, these high energy ions bombard the atoms on the wafer lattice and disorder those atoms that are near the wafer surface.[4] As a result, lots of vacancies and interstitials are created, and an amorphous layer is formed in the vicinity of the wafer surface.[4] To recrystallize the amorphous layer, and to incorporate the dopant atoms into substitutional sites of the lattice, the wafer needs to be annealed at an elevated temperature.

The most commonly used annealing method is rapid thermal annealing (RTA). Some alternatives to RTA are emerging, such as laser annealing and microwave (MW) annealing.[5–8] With RTA, the entire silicon wafer is heated to the annealing temperature.[2,9] This can cause excessive dopant diffusion. In contrast, due to silicon's high optical absorptivity in the visible and near-IR regimes, laser annealing can target just the amorphous region.[10] This minimizes the thermal budget needed for the annealing process. In addition, laser annealing can provide a higher degree of dopant activation than RTA, by overcoming the solid solubility limits for the dopant ions.[11] Microwave annealing also reduces the thermal budget with respect to RTA because dopant activation can be accomplished at a lower annealing temperature.[12] However, microwave annealing is still limited by the solid solubility limits for the dopant ions.

In this study, As^+ implanted Si wafers are annealed by susceptor-assisted microwave and laser annealing. The dopant activation is estimated by measuring the sheet resistance of annealed samples via four-point probe analysis. The extents of recrystallization of the amorphous layers during MW and laser annealing are assessed by ion channeling and Rutherford backscattering spectrometry (RBS). The dopant distributions before and after annealing are studied by secondary ion mass spectrometry (SIMS). Laser annealing shows advantages for dopant activation. The two techniques show the same performance with respect to recrystallization. The dopant depth profiles achieved by MW annealing and laser annealing have different characteristics that make them suitable for different applications. Laser annealing appears to be beneficial for annealing n-wells and p-wells for complementary metal-oxide semiconductor (CMOS) devices. Susceptor-assisted MW annealing is good for annealing source and drain regions in MOSFETs.

[a)]Electronic mail: TA@asu.edu

II. EXPERIMENT

Arsenic ions were implanted into (001) orientated Si wafers that are p-type boron doped. The implantation was performed with an energy of 180 keV and doses of 1×10^{15} and $4 \times 10^{15}\,\mathrm{cm}^{-2}$. To minimize ion channeling during implantation, the wafers were titled at 7° off the incident beam.

MW annealing of the As^+ implanted Si was conducted in a 2.8×10^4 cm^3 cavity MW oven with a 1200 W magnetron source, and using a single frequency of 2.45 GHz. Implanted Si samples were mounted on a SiC susceptor. SiC can efficiently convert the MW energy into heat, and rise to a relatively high temperature, due to its high dielectric loss and strong absorption efficiency for MWs.[9] As a result, the ion-implanted silicon samples on the susceptor were heated by conductive heating from the susceptor.[9,13] Raytek Compact MID series pyrometers (measurable range of 200–1000 °C) were used to monitor the *in situ* sample surface temperature as a function of time. The anneal time varied from 20 to 100 s, and the corresponding temperature ranged from 449 to 815 °C.

The laser annealing was performed on a Universal Laser Systems PLS6MW with a 1.06 μm wavelength fiber laser. The fiber laser had an average output power of 40 W. For the laser annealing experiments, the laser power was modulated from 65% (26 W) to 85% (34 W). The laser beam was focused to a circular spot with a size of 25 μm. The beam was rastered across the ion implanted silicon sample at a speed of 30 cm/s, and at a frequency of 500 kHz.

The extent of dopant activation was estimated by measuring the sheet resistance (R_{sh}) of each sample. The measurements were conducted using a four-point probe system equipped with a 100 mA Keithley 2700 digital multimeter.

The presence of implantation damage in as-implanted Si and the extent of recrystallization in annealed As^+ implanted Si samples were studied by ion channeling based on RBS. Since the As^+ implanted samples are prepared from (001) oriented Si wafers, a 2 MeV He^+ ion beam was aligned along the sample's [001] channeling direction. A channeling spectrum was then obtained by tilting the sample to 5° from the normal and rotating the sample in the azimuth until the yield reached a minimum.

Diffusion of dopants was investigated by comparing depth profiles of arsenic ions before and after the samples were MW or laser annealed. The depth profiles were obtained by SIMS. The primary ion used for SIMS was Cs^+, and secondary 30 Si^+ and 75 As^+ ion signals were alternatively collected as a function of sputtering time. The depth was calibrated by measuring the crater depth, and the concentration was calibrated by equating the area under the profile to the dose of arsenic ions. Using this method, the ion signal as a function of time was converted to an As^+ concentration as a function of depth. The depth values were corroborated using RBS analysis.

III. RESULTS AND DISCUSSION

The output power was varied for the laser anneals, while the annealing time was varied for the MW anneals. For a side by side comparison, the absorbed energy density was calculated for both laser and MW annealing. The resulting sheet resistances of laser annealed and MW annealed samples are compared as a function of absorbed energy density, in Fig. 1. The results show that the laser annealing achieves a similar or even lower sheet resistance while using only ~1/7 of the energy density that is required for the MW annealing. With laser annealing, the sheet resistance of the annealed sample drops abruptly as the energy density is increased. In contrast, once the energy density in the MW annealing is above a threshold, the sheet resistance of the MW annealed samples begins to drop dramatically to a certain level, and then decreases slowly as the energy density increases. Based on the above comparison, laser annealing shows great advantage over MW annealing for dopant activation, since it enables higher levels of dopant activation at a lower energy density.

The high extent of dopant activation, achieved at a lower energy density in laser annealing, is due to surface heating

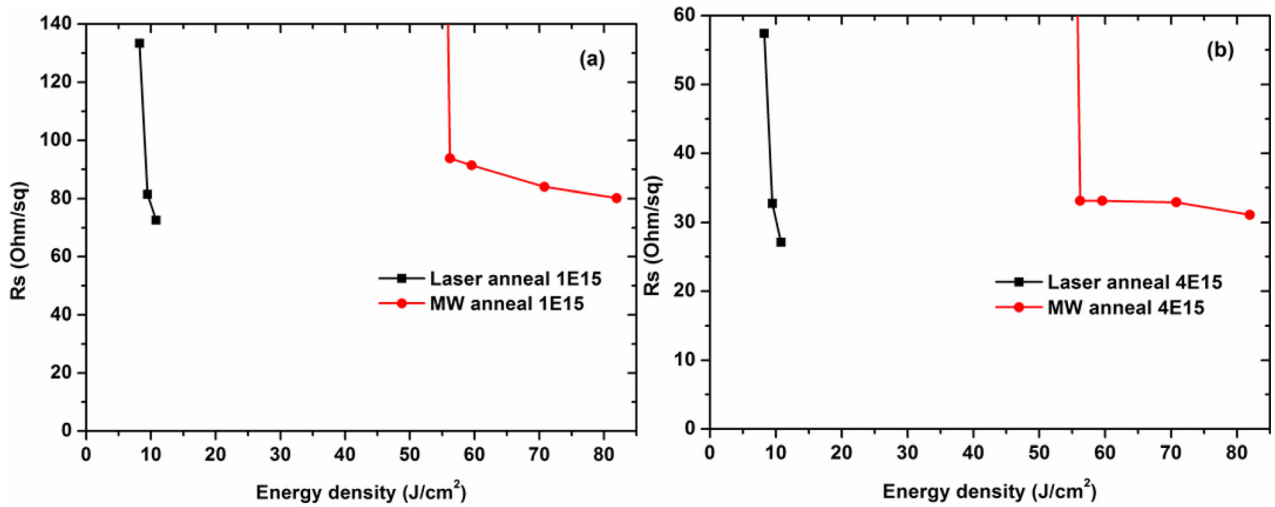

FIG. 1. (Color online) Sheet resistance of As^+ implanted Si after laser annealing with various powers and MW annealing with various times (a) 1×10^{15} As^+ cm^{-2} implanted Si and (b) 4×10^{15} As^+ cm^{-2} implanted Si.

during laser annealing. The amorphous Si has a larger absorption coefficient α ($10^4\,\mathrm{cm}^{-1}$) at a wavelength of 1.06 μm (laser wavelength used in this study).[11] As a result, most of the laser energy is absorbed in the thin amorphous layer as opposed to the crystalline substrate. This causes the Si surface to melt. According to stopping and range of ions in matter simulation, the thickness of the amorphous layer is about 0.24 μm ($2R_p$).[14] Once the laser beam penetrates down to the crystalline Si substrate, the energy density is diluted due to the relative small absorption coefficient α ($50\,\mathrm{cm}^{-1}$) of crystalline Si. The energy absorbed per unit volume (in Joules per cubic centimeter) as a function of sample depth (z) during laser annealing can be calculated by[11]

$$\Phi(z) = I_0[(1-R)/d]e^{-z/d}, \tag{1}$$

where the I_0 is the output/incident energy density of the laser (in Joules per square centimeter), R is the reflectance of Si at the laser wavelength (1.06 μm) and d is the absorption depth, which is the reciprocal of the absorption coefficient α. According to Eq. (1), the absorption depth d could be calculated from the reciprocal of the absorption coefficient, as 1 and 200 μm for amorphous silicon and crystalline silicon, respectively.[11] Note that the absorption depth here denotes a penetration depth at which the magnitude of the laser beam has decayed to $1/e$ of its surface value. Compared to the absorption depth, the 0.24 μm thickness of the amorphous silicon layer is relative small. Therefore, a Φ(z) plot with a near-linear shape was observed rather than an exponential function. This calculated result for the absorbed energy density per unit volume across the sample depth z during laser annealing is shown as the solid black curve in Fig. 2. The energy absorbed per unit volume by the amorphous layer is almost 3 orders of magnitude greater than that absorbed by the crystalline layer.

MW annealing results in volumetric heating.[15] Instead of being mainly absorbed by the amorphous layer, the energy will be absorbed uniformly across the entire Si sample. Therefore, the energy absorbed per unit volume becomes lower (compared to laser annealing) because it is uniformly distributed across the 625 μm thick Si sample. Figure 2 compares the energy absorbed per unit volume as a function of sample depth for laser annealing and MW annealing. The energy distributions across the sample during laser annealing and MW annealing are quite different. Due to the different energy distributions, laser annealing causes liquid phase growth,[11,16] while MW annealing provides solid phase regrowth. These different regrowth processes result in different dopant activation processes. As a consequence, the laser annealing is more efficient in terms of dopant activation.

The annealing process involves not only dopant activation but also the recrystallization of the amorphous layer at the surface. Ion channeling can be used to determine the levels of recrystallization that result from the MW and laser annealing processes.[17] The crystalline material typically results in a low yield of backscattering ions during ion channeling. However, the amorphous material has a high yield of backscattering ions because of the disordered atoms in the layer.[17] Moreover, defects in the material cause dechanneling of the incident ions, and this then leads to an increased yield of backscattering ions.[17] Figure 3 compares the [001] ion channeling spectra of As^+ implanted Si before and after laser annealing.

In Fig. 3, the dramatic decrease of the backscattering ion yield after laser annealing indicates that the amorphous layers are recrystallized during laser annealing. The As^+ peak also drops after laser annealing. This is because the majority of the As^+ ions move from interstitial positions to substitutional positions in the lattice, after annealing. As a result, the probability of the incident ions being backscattered from interstitial As^+ ions is reduced, leading to a reduced yield of backscattering ions for the annealed samples. A slightly higher backscattering ion yield is seen, in the low energy region, for the 75% power laser annealed sample. This might be due to the presence of interstitial point defects

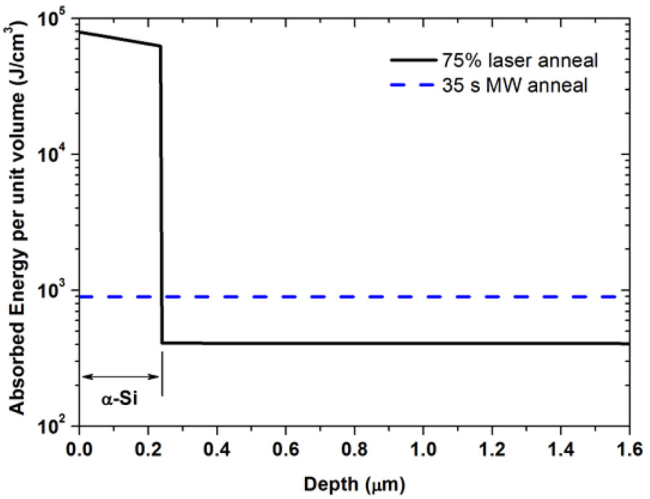

FIG. 2. (Color online) Calculated absorbed energy per unit volume during laser annealing and MW annealing.

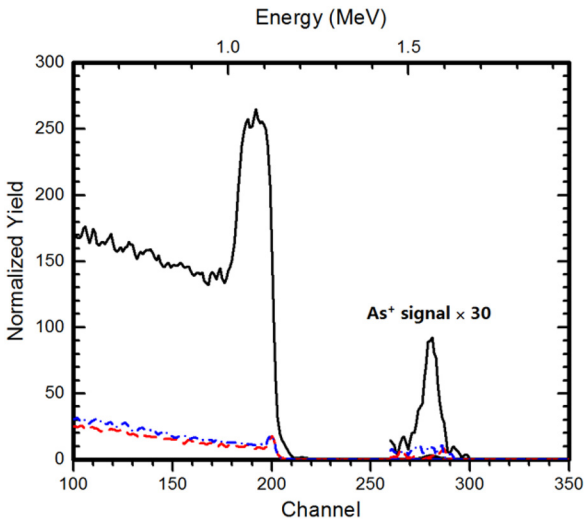

FIG. 3. (Color online) RBS ion channeling spectra in the [001] direction from 1×10^{15} As^+ cm^{-2} implanted Si samples: as-implanted sample (black solid line), 75% power laser annealed sample (blue dashed–dotted line), and 85% power laser annealed sample (red dashed line).

in the sample.[17] Such interstitial point defects might result from inadequate crystal regrowth, since the 75% power laser yields a lower annealing temperature locally, compared to the 85% power laser. This would result in a correspondingly slower mass transportation. These point defects can cause dechanneling of the channeling ions and thereby increase their chance of being backscattered, leading to an increased ion backscattering yield in the low energy region of the spectrum.[17]

Figure 4 compares the ion channeling spectra of 100 s MW annealed and 85% power laser annealed samples. The black line is the backscattering ion yield from an as-implanted sample. After MW and laser annealing, the backscattering ion yield drops. The ion channeling yields immediately after the first surface peak indicate the crystallinity of each sample. In Fig. 4(a), the yields after the two first surface peaks are the same, indicating that the same crystallinity is present, regardless of their extent of dopant activation.

Figure 4(b) shows the yields of the ions that are backscattered from interstitial As^+. These provide a good estimation of dopant activation. The yield of the As^+ peak from the 85% power laser annealed sample is slightly lower than that of the 100 s MW annealed sample. This indicates that there is a slightly lower amount of interstitial As^+ ions and a higher extent of dopant activation in the 85% power laser annealed sample. This fact is supported by the lower sheet resistance of the 85% power laser annealed sample in Fig. 1(a). The 85% power laser annealed sample has a 10% lower sheet resistance than the 100 s MW annealed sample (Fig. 1(a)).

Dopant atoms will typically diffuse under heat treatment. Both the laser and the MW anneals result in heating of the implanted layers. In this study, dopant diffusion is assessed by measuring the depth profiles of As^+ before and after laser and MW annealing via SIMS analysis. Figure 5 shows the depth profiles for the as-implanted, laser annealed, and microwave annealed samples. The profiles show that the laser annealing results in significant dopant diffusion, and that increased power enhances the diffusion. This is due to liquid phase epitaxy in laser annealing.[11] A large portion of the laser energy is absorbed at and near the Si surface as shown in Fig. 2. This high energy input per unit volume of pulsed laser annealing melts the Si surface layer.[11,16] After a typical irradiation of 2×10^{-6} s, the surface recrystallizes quickly at the liquid–solid interface.[11] In the melted layer, the mobility of the dopants is much larger than that in the solid phase. Therefore, dopants are more likely to diffuse and redistribute toward low concentration regions. As a result, the As^+ concentration in the 75% and 85% power laser annealed samples are quite uniform within 200 and 600 nm (from the surface), respectively. The characteristics of such depth profiles are quite suitable for ion implanted n-wells in CMOS technology.

In conventional CMOS processing, n-well and p-well regions are formed by implanting dopants to define the well region first. Then, the ion implanted wafers are annealed in a drive-in furnace to enable diffusion. To control the diffusion depth, and to obtain a uniform distribution of dopants, and to obtain a well depth of 2–3 μm, the thermal cycle is typically 4–6 h at 1000–1100 °C.[3] In contrast, we find that laser annealing can achieve a uniform and deep dopant profile in a much shorter time through liquid phase regrowth. In addition, the diffusion depth that results from laser annealing can be controlled by adjusting the energy output and the wavelength of the laser.[10] However, the energy density distribution in our pulsed laser beam itself is Gaussian. Rastering of the pulsed laser beam across the sample results in slightly nonuniform energy distribution. This in turn results in only 7.5%–10% of maximum difference in Rs across the 1×1 cm Si sample. As a result, laser annealing appears to be an efficient alternative to drive-in furnace annealing for n-well and p-well formation; however, the control of the energy density uniformity during the laser raster must be improved in order

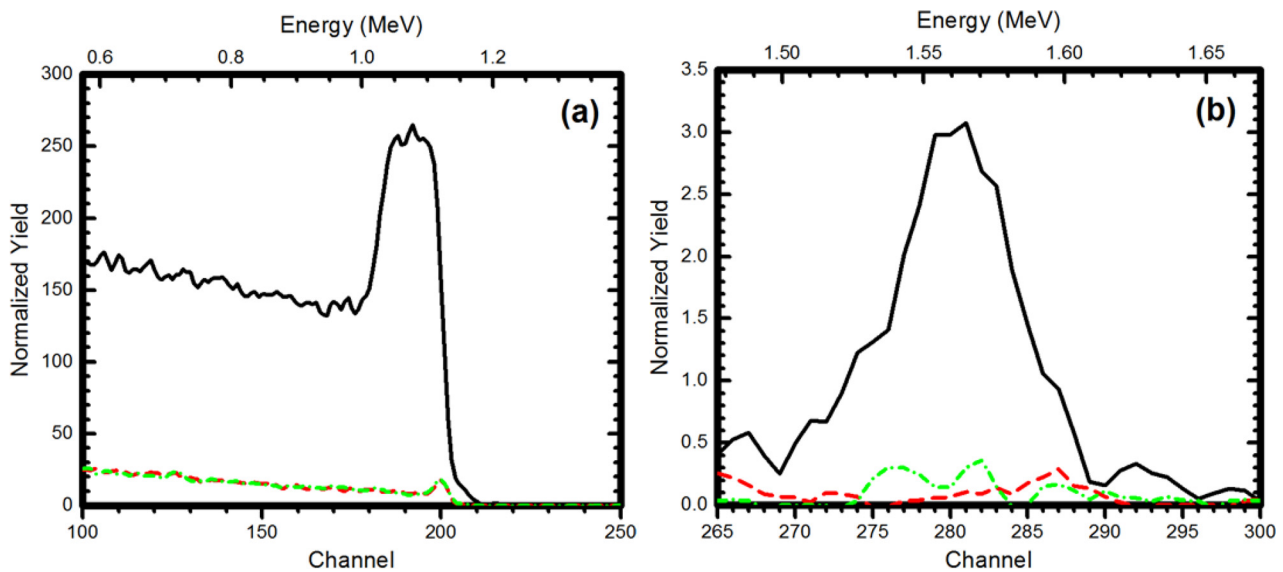

FIG. 4. (Color online) RBS ion channeling spectra in a random and in the [001] direction from 1×10^{15} As^+ cm^{-2} implanted Si samples. (a) Si signal, (b) magnified arsenic signal: as-implanted sample in the [001] direction (black solid line), 100 s MW annealed sample in the [001] direction (green dashed–dotted line) and 85% power laser annealed sample in the [001] direction (red dashed line).

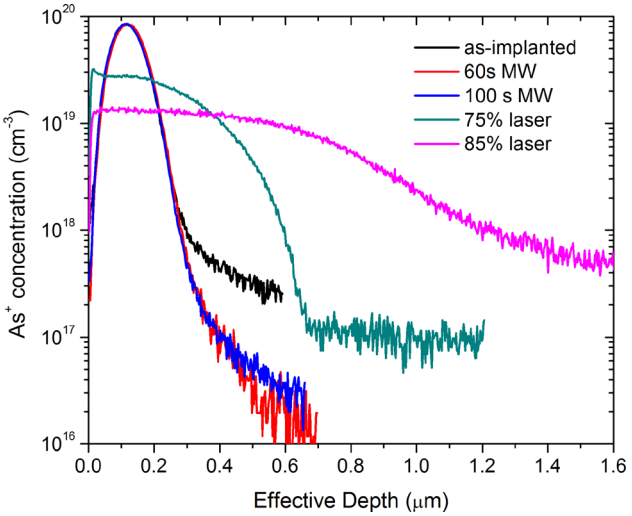

FIG. 5. (Color online) SIMS profile from 1×10^{15} As^+ cm^{-2} implanted Si samples before annealing (as-implanted), and after MW annealing (60 and 100 s) and laser annealing (75% and 85% power).

to achieve necessary uniformity required for large-scale manufacturing.

On other hand, there is no measurable dopant diffusion in the As^+ depth profiles of the MW annealed samples in Fig. 5. In addition, the MW annealing achieves the same extent of dopant activation as laser annealing does. This absence or minimization of diffusion results from the low temperature and short duration of the MW annealing. The highest temperature that is reached during the 60 and 100 s MW annealing is only 706 and 815 °C, respectively. These low temperatures are below the melting point of silicon. This means that solid-phase regrowth occurs during MW annealing. During solid-phase regrowth, dopant atoms are only able to diffuse to nearby atom sites, with the help of lattice distortion and vibration. This minimizes long range diffusion. As a result, MW annealing is a suitable technique for annealing ion implanted source, drain, and channel regions (that require minimized dopant diffusion) for MOSFET fabrication.

IV. CONCLUSION

Our study shows that laser annealing has advantages for dopant activation when compared to MW annealing. The laser anneal is beneficial for deep well formation with a uniform dopant concentration. The relatively high diffusion depth that is observed for laser annealing can be addressed by choosing a shorter wavelength laser.[10] The shorter wavelength will have a lower penetration depth into the silicon, thereby reducing the depth of the surface melting.[10] The minimization of diffusion that is achieved by MW annealing provides a marked benefit for shallow junction devices.

ACKNOWLEDGMENTS

The authors thank N. David Theodore in NXP Semiconductors N.V. for his great help in editing this manuscript. This work was partially supported by National Science Foundation (C. Ying, Grant No. DMR-0902277) to whom the authors are greatly indebted.

[1]T. L. Alford, D. Thompson, J. Mayer, and N. D. Theodore, J. Appl. Phys. **106**, 114902 (2009).
[2]R. N. Vemuri, M. J. Gadre, N. Theodore, W. Chen, S. Lau, and T. L. Alford, J. Appl. Phys. **110**, 034907 (2011).
[3]J. D. Plummer, *Silicon VLSI Technology: Fundamentals, Practice, and Modeling* (Prentice Hall, Upper Saddle River, 2000).
[4]J. Mayer and S. Lau, *Electronic Materials Science: For Interconnection Circuits in Si and GaAs* (Macmillan, New York, 1990).
[5]A. Gat, J. Gibbons, T. Magee, J. Peng, V. Deline, P. Williams, and C. Evans, Jr., Appl. Phys. Lett. **32**, 276 (1978).
[6]A. Murakoshi, T. Harada, K. Miyano, H. Harakawa, T. Aoyama, H. Yamashita, and Y. Kohyama, Jpn. J. Appl. Phys., Part 1 **55**, 046501 (2016).
[7]T. J. Michalak, J. Herman, A. Basavalingappa, M. Rodgers, D. França, and C. Borst, J. Vac. Sci. Technol., B **33**, 011201 (2015).
[8]S. Paul, W. Lerch, J. Chan, S. McCoy, J. Gelpey, F. Cristiano, F. Severac, P. Fazzini, and D. Bolze, J. Vac. Sci. Technol., B **26**, 293 (2008).
[9]S. Fong, C. Wang, T. Chang, and T. Chin, Appl. Phys. Lett. **94**, 102104 (2009).
[10]M. A. Green and M. J. Keevers, Prog. Photovoltaics: Res. Appl. **3**, 189 (1995).
[11]J. Poate, *Laser Annealing of Semiconductors* (Academic, London, 1982).
[12]Z. Zhao, N. D. Theodore, R. N. Vemuri, S. Das, W. Lu, S. Lau, and T. L. Alford, Appl. Phys. Lett. **103**, 192103 (2013).
[13]M. Damm and C. O. Kappe, Mol. Diversity **13**, 529 (2009).
[14]"Interactions of ions with matter," http://www.srim.org/, accessed November 2013.
[15]D. E. Clark and W. H. Sutton, Annu. Rev. Mater. Sci. **26**, 299 (1996).
[16]P. Baeri, S. Campisano, G. Foti, and E. Rimini, Appl. Phys. Lett. **33**, 137 (1978).
[17]L. C. Feldman, J. W. Mayer, and S. T. Picraux, *Materials Analysis by Ion Channeling: Submicron Crystallography* (Academic, New York, 1986).